

Modeling electronic, mechanical, optical and thermal properties of graphene-like BC₆N materials: Role of prominent BN-bonds

Nzar Rauf Abdullah^{a,b}, Hunar Omar Rashid^a, Chi-Shung Tang^c, Andrei Manolescu^d, Vidar Gudmundsson^e

^aDivision of Computational Nanoscience, Physics Department, College of Science, University of Sulaimani, Sulaimani 46001, Kurdistan Region, Iraq

^bComputer Engineering Department, College of Engineering, Komar University of Science and Technology, Sulaimani 46001, Kurdistan Region, Iraq

^cDepartment of Mechanical Engineering, National United University, 1, Lienda, Miaoli 36003, Taiwan

^dReykjavik University, School of Science and Engineering, Menntavegur 1, IS-101 Reykjavik, Iceland

^eScience Institute, University of Iceland, Dunhaga 3, IS-107 Reykjavik, Iceland

arXiv:2003.08467v1 [cond-mat.mes-hall] 18 Mar 2020

Abstract

We model monolayer graphene-like materials with BC₆N stoichiometry where the bonding between the B and the N atoms plays an important role for their physical and chemical properties. Two types of BC₆N are found based on the BN bonds: In the presence of BN bonds, an even number of π -bonds emerges indicating an aromatic structure and a large direct bandgap appears, while in the absence of BN bonds, an anti-aromatic structure with an odd-number of π -bonds is found resulting a direct small bandgap. The stress-strain curves shows high elastic moduli and tensile strength of the structures with BN-bonds, compared to structures without BN-bonds. Self-consistent field calculations demonstrate that BC₆N with BN-bonds is energetically more stable than structures without BN-bonds due to a strong binding energy between the B and the N atoms, while their phonon dispersion displays that BC₆N without BN-bonds has more dynamical stability. Furthermore, all the BC₆N structures considered show a large absorption of electromagnetic radiation with polarization parallel to the monolayers in the visible range. Finer detail of the absorption depend on the actual structures of the layers. A higher electronic thermal conductivity and specific heat are seen in BC₆N systems caused by hot carrier-assisted charge transport. This opens up a possible optimization for bolometric applications of graphene based material devices.

Keywords: Energy harvesting, Thermal transport, Graphene, Density Functional Theory, Electronic structure, Optical properties, and Stress-strain curve

1. Introduction

Material structures at the nanoscale with a combination of carbon atoms, C, with its neighboring Boron, B, and Nitrogen, N, atoms in the periodic table forming BCN [1], BC₃N [2], and BC₆N [3] have shown interesting physical properties and lead to numerous potential technological applications in the fields of lithium ion batteries [4], electrocatalysis [5], sensors [6], nano-electronics devices, optical devices [7], and field emission.

Experiments and calculations found that the physical properties of B_xC_yN_z depend on the concentration of B, C, and N atoms in the lattice [8, 9]. For instance, the stress-strain characteristics of BC₆N have shown anisotropy in the mechanical response when uniaxial tensile simulations were conducted along the armchair and the zigzag directions [3]. In addition, increasing the thickness of BC₆N results in a decreased bandgap, and the application of a perpendicular electric field decreases the bandgap even

more. Semiconductor to insulator transition is thus found [10]. The bandgap opening can be tuned by the concentration ratio of B and N atoms, in which the variation of the bandgap with the B and N dopant concentration is almost linear [11].

It has been found that the inversion symmetry breaking of BC₆N with high carrier mobility leads to a pair of inequivalent valleys with opposite Berry curvatures in the vicinities of vertices [12]. This leads to a direct bandgap with 1.833 eV, which is beneficial for realization of a valley Hall effect [12].

One of the important optical characteristics of graphene is its capability to function as an absorbent for a wide range of electromagnetic radiation [13]. The optical study of graphene and related materials is important for understanding their electronic structures and excitation spectra. Consequently, there are many potential applications of optical and photonic effects in which graphene has been used [14, 15, 16, 17]. The sensitivity of the electronic properties of graphene to electromagnetic adsorption indicates a very good candidate for photonic application such as sensors [18], and the low electron energy loss spectroscopy

Email address: nzar.r.abdullah@gmail.com (Nzar Rauf Abdullah)

(EELS) allows graphene to be used for detecting changes in the electronic structure with a high spatial resolution [19]. BC₆N also presents highly promising optical characteristics while individual B or N doping of graphene does not significantly influence the absorption spectra. However, significant red shift in absorption towards the visible range of the radiation at high BN doping is found to occur [20].

Thermoelectric measurements of BC₆N show that the material behaves as a p-type or an n-type semiconductor with a high Seebeck coefficient of 300 $\mu\text{V}/\text{K}$ at room temperature [21]. It has also been revealed that the B_xC_yN_z system marks up to a 20 times larger Seebeck coefficient than pure graphene [22].

To alter the properties of pure graphene, we investigate a substitutional BN codoping, due to the radii similarity between them and C, along with the resultant BC₆N semiconductor. The main idea in this work is the effect of the bonding between the B and N dopants in the BC₆N on its physical characteristics. We analyze the electronic, the mechanical, the optical, and the thermal characteristics, depending on the composition and the atomic arrangement of the B, C, and N atoms in the lattice. In addition, we investigate the stability of the resulting structures, and how the internal interaction energies influence their properties. We observe to which extent the BN co-doping positions within the graphene sheets modify all their physical characteristics.

In Sec. 2 the structure of BC₆N nanosheet is briefly overviewed. In Sec. 3 the main achieved results are analyzed. In Sec. 4 the conclusion of the results is presented.

2. Model and Computational Details

We perform first-principle calculations on monolayer BC₆N nanosheets using the Perdew-Zunger (PZ) exchange-correlation functionals [23]. Norm-conserving pseudopotential is used in the current work [24] with a kinetic energy cutoff 10 eV. The atomic positions are fully optimized by implementing a quasi-Newton algorithm for atomic force relaxation. The structure is relaxed until the total force on each atom is less than 0.02 eV/Å and the mesh grid of the atomic force relaxation is 12 × 12 × 1. All calculations are performed using the Kohn-Sham version of the Density Functional Theory (DFT) [25] implemented in the Quantum Espresso (QE) package [26, 27]. We consider a large vacuum interval, 20 Å, between the periodic slabs of BC₆N to avoid interaction between adjacent layers.

For each structure, the integration over the Brillouin zone was calculated by QE on an 8 × 8 × 1 grid, using Bloch's theorem for the Self Consistent Field (SCF) calculation. Then a denser mesh-grid of 100 × 100 × 1 was used for the density of states (DOS) calculations, and the band structure was calculated along a smooth path along (Γ-K-M-Γ). In addition, XCrySDen, a crystalline and molecular structure visualization program, is used for visualization of the results of our models [28].

In order to explore the optical properties of the system, we calculate the dielectric tensor with QE using the energy interval from 0 to 20 eV. The imaginary part uses the response function derived from a perturbation theory with adiabatic tuning, while the real part is evaluated using the Kramers-Kronig transformation [29].

Consequently, we analyze the post-processed results from the QE with the Boltzmann transport properties (BolzTraP) package which calculates the semi-classic transport coefficients [30]. We can thus calculate the electronic thermal conductivity, electric conductivity, and specific heat [31, 32].

3. Results

In this section, our main results for pristine and BN-codoped graphene forming BC₆N are shown. After modeling a pure graphene (PG) structure, we constructed a BN-codoping within the graphene to make three configurations of BC₆N: B is fixed at the ortho position (blue color) and N is put at the meta, or the para position (red color) with respect to B, as shown in Fig. 1. In the first doped structure, it is assumed that there is bonding between B and N atoms (BN-bond) which is identified as b-BNG here (Fig. 1(b)). Furthermore, assuming there is no BN-bond in the structure, we consider one (two) carbon atom(s) located between the B and the N atom, identified as nonb-BNG-1 and nonb-BNG-2, respectively. The number 1 and 2 here refers to the number of carbon atom(s) between the B and the N atom in the clockwise direction. The relative positions of the B and N around all the C hexagon is a key factor for the physical properties of the doped graphene. As we know, each carbon atom has 4 electrons in the outer-shell (out of 6), 3 are bonded with neighboring atoms (σ -electrons) and the 4th electron (a delocalized π -electron) which is above and below the honeycomb, contributes to conduction, and the π -orbitals overlap, strengthening the bonding. The highly mobile π -electrons act as mass-less fermions that satisfies the Dirac equation.

The lattice constants of b-BNG, nonb-BNG-1, and nonb-BNG-2 nanosheets are approximately equal to 4.855, 4.851, and 4.853 Å, respectively. In the case of b-BNG, the average lengths of the C-C, the C-B and the C-N bonds are found to be 1.393, 1.442 and 1.378 Å, respectively. For nonb-BNG-1, the average bond length of C-C, C-B and C-N bond lengths are 1.395, 1.430 and 1.389 Å, respectively. In the last doped structure, nonb-BNG-2, the average bond lengths of C-C, C-B and C-N bond are 1.381, 1.4302 and 1.411 Å, respectively. The bond lengths between the C, N and B atoms will help to understand better the mechanical properties of the BC₆N nanosheets as will be shown later. The number of C-C, C-B, C-N, and B-N bonds in a nanosheet will also influence the stability of the structure.

In order to understand better the bonding between the C, B, and N atoms, we provide the electron localization

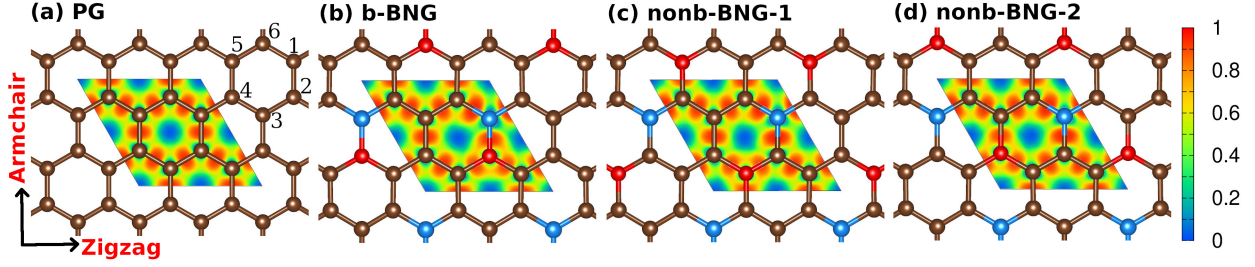


Figure 1: Pure graphene (PG) nanosheet (a), and b-BNG (b), nonb-BNG-1 (c) and nonb-BNG-2 (d) nanosheets where the C atoms are brown, B atoms are blue, and N atoms are red. The contour plots demonstrate the electron localization function (ELF). The numbers from 1 to 6 display the position of atoms in the hexagon. The positions 1, 2, and 3 in the hexagon are called ortho-, meta-, and para-position, respectively.

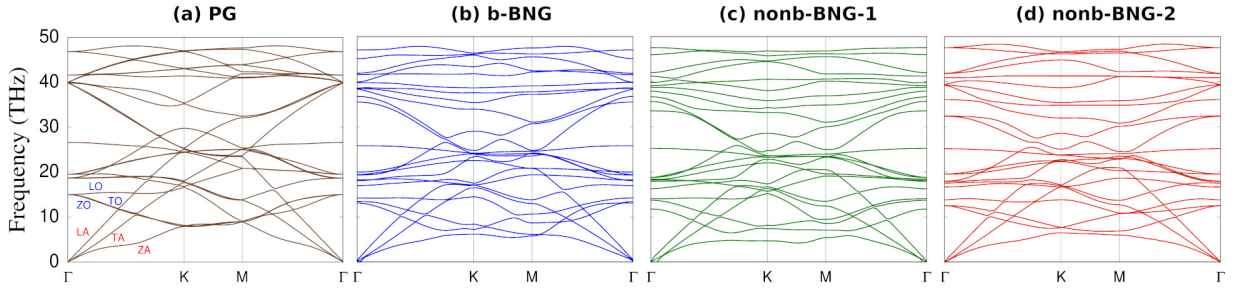


Figure 2: The calculated phonon band structure of PG (a), b-BNG (b), nonb-BNG-1 (c), and nonb-BNG-2 (d) structures along high symmetry of first Brillouin zone.

function (ELF) in Fig. 1 (contour plot) [33]. A high ELF on a particular bond indicates a greater stiffness or rigidity of that bond. The ELF is high for the C-C bonds in PG. In addition, it is higher for a C-N bond compared to a C-B bond in a BN-codoped graphene structures [34].

3.1. Structural stability

The binding energies of C-B and C-N are smaller than those of C-C and B-N. The more stable structure will thus have a lesser number of C-B and C-N bonds in the nanosheets [35]. Therefore, the b-BNG is a relatively more stable structure than the nonb-BNG because of fewer C-B and C-N bonds in b-BNG. This observation shows the BN bond is more stable than the BC or the NC bond. Total energy calculations are utilized to study the structure stability. Our DFT calculations show that the formation energy of the b-BNG structure is -191.721 eV which is relatively smaller than that of the nonb-BNG-1, -190.533 eV, and the nonb-BNG-2, -190.644 eV. This demonstrates that b-BNG is energetically more stable than a nonb-BNG structure.

3.2. Interaction energy

The interaction energy of each considered structure can be obtained from the total energy [31]. The SCF calculations of our systems show that the b-BNG structure has a higher attractive interaction comparing to the nonb-BNG structures. This would be expected because the distance between the B and N atoms in b-BNG, the bonding length

of B-N with 1.411 Å, is small compared to the distance between the B and N atoms in nonb-BNG-1 with 2.432 Å, and nonb-BNG-2 with 2.802 Å.

3.3. Dynamic stability

The dynamic stability of BC_6N nanosheets can be checked by calculating the phonon dispersion relations presented in Fig. 2 for the PG (a), b-BNG (b), nonb-BNG-1 (c) and nonb-BNG-2 (d). In general, the phonon dispersion of a unit-cell of graphene containing two atoms at A and B positions consists of six modes: Three acoustic and three optical modes. Our $2 \times 2 \times 1$ graphene supercell consists of 8 atoms leading to 24 modes in the phonon band structure.

The acoustic modes of PG represented by ZA, TA, and LA (the lowest three modes) are isotropic for the long waves ($q \rightarrow \Gamma$) which is required for the symmetry characteristics of pure graphene [36]. The next three modes represented by ZO, TO and LO are optical modes. In PG, the LO/TO at Γ , LO/LA at K and ZO/ZA at K are double degenerate indicating the symmetry of the unit cell. In the three forms of the BC_6N structures here, we found that these modes are split, which demonstrates the symmetry breaking of the crystal.

The positive values of the phonon band structure of PG and nonb-BNG2-2 indicate the more dynamically stable structures of the nanosheets, while very small negativity in ZA mode of the b-BNG and the nonb-BNG-1 show relatively less dynamically stable structures. The ZA is the

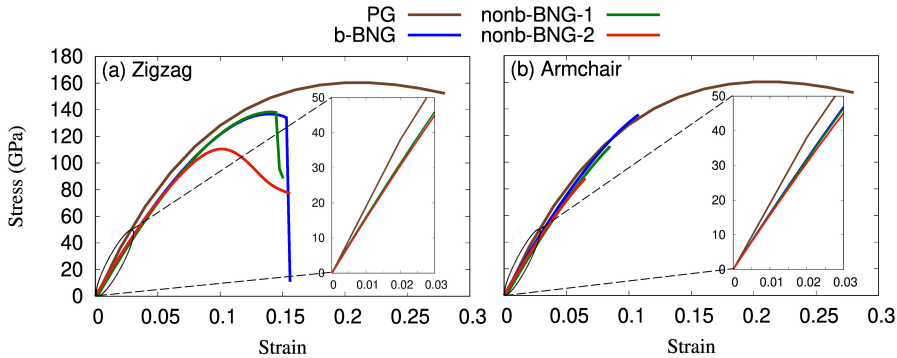


Figure 3: Stress-strain curves for PG (brown), b-BNG (blue), nonb-BNG-1 (green), and nonb-BNG-2 (red) in the zigzag (a) and the armchair (b) direction. The inset shows linear and elastic region of stress-strain curve.

main mode responsible for the lattice thermal conductivity in the system [37].

3.4. Mechanical properties

To calculate the mechanical behavior, the fully relaxed simulation cell is exposed to a uniaxial tensile load of a constant strain rate. The stress-strain curves for three BC_6N structures are plotted together with the one for the PG in Fig. 3 for the x -, the zigzag, (a) and the y -, the armchair direction (b).

It can be clearly seen that the linear elastic regime for pure graphene (brown) ends at $\approx 2\%$ (see inset of Fig. 3), where the stress-strain relation becomes nonlinear for both load directions. In the all BC_6N structures, the stress is linearly proportional to strain up to $\approx 3\%$, and becomes nonlinear beyond 3% for both the zigzag and the armchair directions. In the linear regime the samples have elastic characteristics and both the pure and the BC_6N structures undergo only elastic deformations. We notice that the pure graphene sample has a much higher failure strain of 28% with stress ≈ 152 GPa in both directions. The failure strain of PG is in agreement with other stress-strain curve calculations done by molecular dynamics simulations [38] and experimental results [39]. The falling parts of blue, green and red lines, indicate a generation of cracks forming in the doped structures. The initial softening of the red curve indicates a higher ability of stretching in the structure before the fracture point is reached [40].

The BC_6N structures all fail between 14% and 17% strain with stress between 76 to 138 GPa in the zigzag direction, while in the armchair direction they fail between 6.5% and 10% with an ultimate stress 88 and 136 GPa. This indicates that b-BNG has larger internal stress than non-BNG due to the BN-bonds in the armchair direction and relatively high stress in the zigzag direction.

We notice that the stress-strain curves of the three BC_6N samples are almost identical at the failure strain in the zigzag direction, and the ultimate strength among the three samples differs by less than 5%. Furthermore, the three BC_6N samples are different at the failure strain in the armchair direction. This is a convincing evidence

that our sample size is sufficiently large to be statistically representative.

3.5. Electronic Properties

In this section, we focus on the electronic band structure. The length of the B-N bond is slightly greater than the C-C bond length leading to a good doped system with minimal internal stress, but the presence of the B-N together with the C-B and the C-N bonds in the graphene structure breaks the inversion symmetry leading to the opening of a band gap. At the same time, the bonding between the C, B and N atoms in the graphene structure plays an important role in the electronic characteristics. It means that the relative positions of the B and N around all the C hexagon influence the bandgap as is shown in Fig. 4, where the band structure of the PG (a), b-BNG (b), nonb-BNG-1 (c), and nonb-BNG-2 (d) are presented. As expected, the band structure of the PG has a vanishing bandgap between the valence and conduction bands at the K-point. It thus shows the semiconductor behavior of PG with a vanishing gap.

It can be seen from Fig. 4 that the bandgap of b-BNG and nonb-BNG-2 is larger than that of nonb-BNG-1. This can be explained by the aromaticity which introduces a charge delocalization in the BC_6N structures. In b-BNG and nonb-BNG-2, an even number of π -bonds are found which indicates aromatic system while nonb-BNG-1 is anti-aromatic structure with an odd-number of π -bonds. Interestingly, band gap tuning has been attained for graphene systems with adsorbed higher aromatic molecules [41].

Another method for opening a bandgap is the application of the Diels-Alder reaction (DA reaction) which introduces a covalent modification of graphene. In the b-BNG and nonb-BNG-2 where the B and N atoms are substitutionally doped at the 1,2 or 1,4 positions of the hexagon, the DA reaction leads to the simultaneous transformation of a pair of sp^2 carbons in the honeycomb lattice to either 1,2- or 1,4- sp^3 carbon centers, an AD reaction. Therefore, a structure with the π -electrons at neighboring C-atoms confined to local C-C π -bonds in the b-BNG and

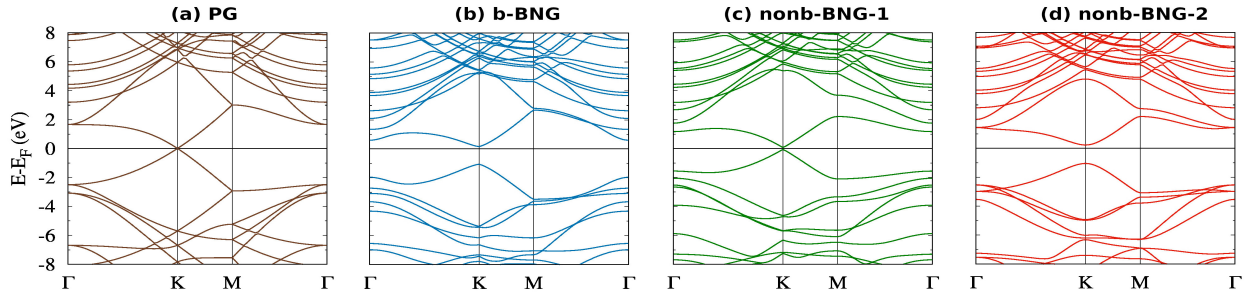


Figure 4: Band structures of PG (a), b-BNG (b), nonb-BNG-1 (c), and nonb-BNG-2 (d) with 0, 1.209, 0.133, 1.273 eV bandgap, respectively. The Fermi energy is set to zero.

nonb-BNG-2 structures are found [42]. This opens up a bandgap [43]. In addition, the strong polarity of the BN bonds in b-BNG may widen the bandgap. In the nonb-BNG-1 structure, the B and N atoms located at position 1 and 3 of the hexagon, imply two all-C segments, each with an odd number of π -electrons, in the hexagons leading to a very small bandgap [42, 44, 45]. These transformations of the covalent bonds are called sublattice symmetry breaking that opens up the bandgap [46]. Our results indicate that both the valence band maxima (VBM) and conduction band minima (CBM) of b-BNG, nonb-BNG-1 and nonb-BNG-2 occur at the K-point, resulting a direct bandgap with 1.209, 0.133, 1.273 eV, respectively.

3.6. Optical Properties

It is well known that the optical properties of graphene do vary with the number of layers. For instance, monolayer graphene can absorb light over a wide range of frequencies. The imaginary part of the dielectric function, ϵ_i , representing the absorption spectra is presented in Fig. 5(a-d) for the aforementioned structures shown in Fig. 1, with the electric field parallel, E_x , (solid line) or perpendicular, E_z , (dashed line) to the plain structure. In order to explain the origin of the peaks in ϵ_i , as contributions of specific transitions between bands, we present in Fig. 5(e-h) the density of states for the corresponding four structures. The location of the most important transitions is approximately indicated in the figures of DOS by golden arrows.

In the case of the PG (brown color), two expected peaks in the complex dielectric function for parallel electric field are observed (solid brown line) at 4.16 and 14.59 eV corresponding to the $\pi \rightarrow \pi^*$ and $\sigma \rightarrow \sigma^*$ transitions, respectively. The first peak has been confirmed experimentally at 4.5 eV using spectroscopic ellipsometry analysis [47]. The slight shift in the first peak in our result can be attributed to the neglect of the interaction between the graphene film and the substrate. In addition, the position of the second peak at 14.59 eV in our calculation is very close to the experimental result at 14.6 eV for free-standing graphene films [48]. The intensity ratio of these two peaks is $\epsilon_{i,L}/\epsilon_{i,R} = 3.015/1.778 = 1.695$ as is expected for monolayer graphene. The intensity ratio indicates that

the $\pi \rightarrow \pi^*$ transition is stronger than the $\sigma \rightarrow \sigma^*$ transition. In the presence of a parallel electric field (brown dashed line) two peaks at 11.46 and 14.83 eV are found corresponding to the $\pi \rightarrow \sigma^*$ and the $\sigma \rightarrow \pi^*$ transitions, respectively.

In the BC_6N structures the rates of the transitions are changed due to the modification of the band structures. In the case of b-BNG and nonb-BNG-2, when there is a large bandgap, the $\pi \rightarrow \pi^*$ peak is shifted to 1.203 and 1.44 eV in the case of parallel electric field, respectively. The second peak is slightly smeared out and located at 3.36 and 4.41 eV for b-BNG and nonb-BNG-2, respectively, indicating a weaker $\sigma \rightarrow \sigma^*$ transition. We note that the first peak in b-BNG and nonb-BNG-2 is located in the visible region. It demonstrates that these BC_6N monolayers have an enhanced visible-light absorption in comparison with graphene, which potentially can be important for photovoltaic applications. The peak shift was found before for the same size of supercell in the case of parallel electric field at 1.11 and 1.39 eV for b-BNG and nonb-BNG-2 [3]. This shift in the transition has also been reported for a larger supercell of BN-codoped graphene with doped ratio of 25% which corresponds to the same doping ratio as in our supercell [20]. It has been shown that the visible-light absorption vanishes at the low ratio of BN-doping [20].

Finally, the first peak indicating the $\pi \rightarrow \pi^*$ transition of nonb-BNG-1 is slightly shifted due to a small bandgap as is shown in Fig. 5(c).

3.7. Thermal Properties

In this section, electronic thermal conductivity, k_e , and specific heat, c , of the aforementioned four structures are presented in the temperature range of $T = 20 - 140$ K. Boltzmann equation implemented in the BoltzTraP software package is used to calculate both k_e and c near the charge neutrality point [49]. In this temperature range, the electron and the lattice temperatures are decoupled for low dimensional graphene structures [50, 51] and the rate of energy transferred between the charge carriers and the acoustic phonons is thus very small. We therefore focus on the regime where the Fermi energy, $\mu \gg k_B T$ and $k_e \propto \sigma_e$, where σ_e is the electrical conductivity.

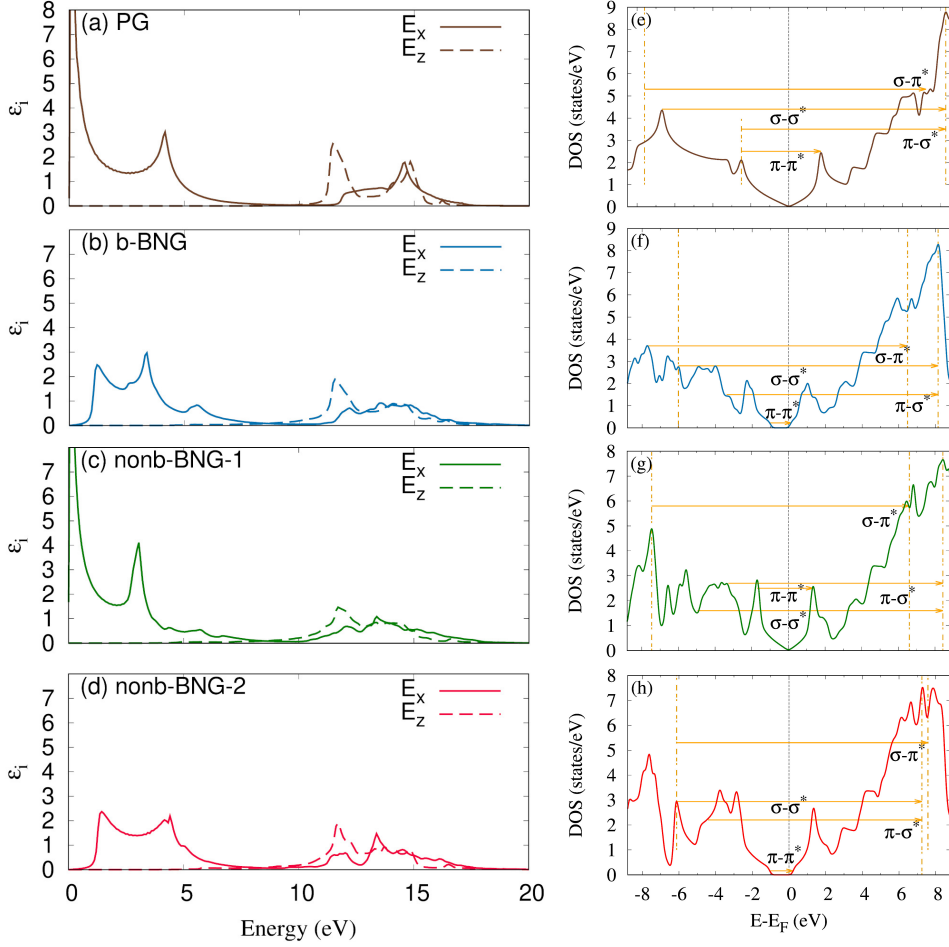


Figure 5: Imaginary part of dielectric function of PG (a), b-BNG (b), nonb-BNG-1 (c), and nonb-BNG-2 (d). Density of states for PG (e), b-BNG (f), nonb-BNG-1 (g), and nonb-BNG-2 (h).

The investigation of k_e defines how the Dirac charge carriers carry energy. This helps us to understand the efficiency of charge harvesting in graphene optoelectronic devices [52]. Electron thermal conductivity (a), electrical conductivity (b), and specific heat (c) are presented in Fig. 6 for PG (brown), b-BNG (blue), nonb-BNG-1 (green), and nonb-BNG-2 (red) near the charge neutrality point. The electron thermal conductance increases proportionally to T^2 with temperature [53]. According to our calculations, the electronic thermal conductivity of b-BNG and nonb-BNG-2 is much larger than that of PG and nonb-BNG-1. This is attributed to the presence of a larger bandgap in b-BNG and nonb-BNG-2 in which hot carrier-assisted charge transport and the electric conductivity is thus increased with temperature as is seen in Fig. 6(b).

The higher electronic thermal conductivity indicates that when a charge carrier is excited by a thermal gradient, it can travel a larger distance and excite additional carriers before it thermalizes with the lattice. Furthermore, a tunable electronic thermal conductivity implies a tunable electronic specific heat (see Fig. 6c) which could be used to optimize bolometric applications of graphene. It thus may have applications in thermoelectric technologies

[54, 55, 56, 57].

4. Conclusion

In this work, we have analyzed the electronic, stress-strain relations, the energy stability, the dynamic stability via phonon dispersion, the optical and the thermal properties of BN-bonded and non-bonded BC_6N structures. We have seen that the bandgap can be tuned by controlling the BN-bonds in the BC_6N structures depending on the electron delocalization processes via the aromaticity of the structure. The presence of BN-bonds promotes the BC_6N structure to a hard material which can withstand large strain. The anisotropy of the mechanical properties depend on the number of C-C, C-N, C-B, and B-N bonds in the structures. We demonstrate that energy stability, dynamic stability, and interaction energy depends on the BN-bonds and show that the graphene-like BC_6N with BN-bonds is the most stable among all studied atomic configuration structures. Furthermore, a high intensity peak in the dielectric function representing the absorption spectra in the visible range was observed in BC_6N structures with a large bandgap depending on the number of

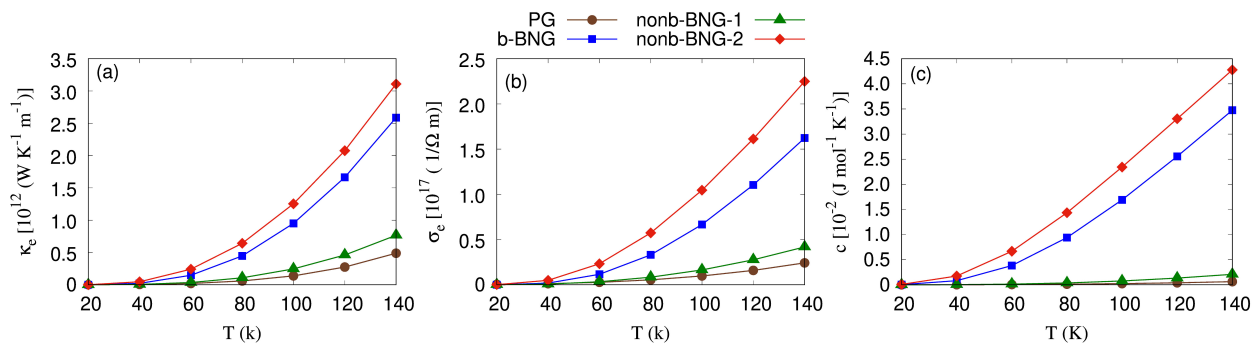


Figure 6: Electronic thermal conductivity (a), electronic conductivity (b), and specific heat (c) are plotted for PG (brown), b-BNG (blue), nonb-BNG-1 (green), and nonb-BNG-2 (red) near charge neutrality point.

π -bonds. This may induce novel optical behavior in which BC_6N can be potentially used in optoelectronic devices. Finally, the electronic thermal conductivity and the specific heat show an outstanding performance of BC_6N with a large bandgap. Therefore, it can be used in thermoelectric devices.

5. Acknowledgment

This work was financially supported by the University of Sulaimani and the Research center of Komar University of Science and Technology. NRA would like to thank Swara Jalal for fruitful discussions. The computations were performed on resources provided by the Division of Computational Nanoscience at the University of Sulaimani.

References

- [1] Angel Rubio. Nanoscale patchworks. *Nature Materials*, 9(5):379–380, 2010.
- [2] C N R Rao and U V Waghmare. *2D Inorganic Materials beyond Graphene*. WORLD SCIENTIFIC (EUROPE), 2017.
- [3] Bohayra Mortazavi, Masoud Shahrokhi, Mostafa Raeisi, Xiaoying Zhuang, Luiz Felipe C. Pereira, and Timon Rabczuk. Outstanding strength, optical characteristics and thermal conductivity of graphene-like bc3 and bc6n semiconductors. *Carbon*, 149:733 – 742, 2019.
- [4] Arava Leela Mohana Reddy, Anchal Srivastava, Sanketh R. Gowda, Hentej Gullapalli, Madan Dubey, and Pulickel M. Ajayan. Synthesis of nitrogen-doped graphene films for lithium battery application. *ACS Nano*, 4(11):6337–6342, 2010. PMID: 20931996.
- [5] Shuangyin Wang, Shuangyin Wang, Lipeng Zhang, Zhenhai Xia, Ajit Roy, Dong Wook Chang, Jong-Beom Baek, and Liming Dai. Bcn graphene as efficient metal-free electrocatalyst for the oxygen reduction reaction. *Angewandte Chemie (International ed. in English)*, 51(17):42094212, April 2012.
- [6] Sumit Beniwal, James Hooper, Daniel P. Miller, Paulo S. Costa, Gang Chen, Shih-Yuan Liu, Peter A. Dowben, E. Charles H. Sykes, Eva Zurek, and Axel Enders. Graphene-like boroncarbon-nitrogen monolayers. *ACS Nano*, 11(3):2486–2493, 2017. PMID: 28165713.
- [7] Sunil Kumar, N. Kamaraju, K.S. Vasu, Angshuman Nag, A.K. Sood, and C.N.R. Rao. Graphene analogue bcn: Femtosecond nonlinear optical susceptibility and hot carrier dynamics. *Chemical Physics Letters*, 499(1):152 – 157, 2010.
- [8] Z. Weng-Sieh, K. Cherrey, Nasreen G. Chopra, X. Blase, Yoshiyuki Miyamoto, Angel Rubio, Marvin L. Cohen, Steven G. Louie, A. Zettl, and R. Gronsky. Synthesis of $\text{b}_x\text{c}_y\text{n}_z$ nanotubules. *Phys. Rev. B*, 51:11229–11232, Apr 1995.
- [9] Angel Rubio, Jennifer L. Corkill, and Marvin L. Cohen. Theory of graphitic boron nitride nanotubes. *Phys. Rev. B*, 49:5081–5084, Feb 1994.
- [10] A. Bafekry. Graphene-like bc6n single-layer: Tunable electronic and magnetic properties via thickness, gating, topological defects, and adatom/molecule. *Physica E: Low-dimensional Systems and Nanostructures*, 118:113850, 2020.
- [11] Pooja Rani and V. K. Jindal. Stability and electronic properties of isomers of b/n co-doped graphene. *Applied Nanoscience*, 4(8):989–996, Nov 2014.
- [12] Xiaobiao Liu, Xikui Ma, Han Gao, Xiaoming Zhang, Haoqiang Ai, Weifeng Li, and Mingwen Zhao. Valley-selective circular dichroism and high carrier mobility of graphene-like bc6n. *Nanoscale*, 10:13179–13186, 2018.
- [13] F. Marra, J. Lecini, A. Tamburrano, L. Pisu, and M. S. Sarto. Electromagnetic wave absorption and structural properties of wide-band absorber made of graphene-printed glass-fibre composite. *Scientific Reports*, 8(1):12029, 2018.
- [14] Kian Ping Loh, Qiaoliang Bao, Goki Eda, and Manish Chhowalla. Graphene oxide as a chemically tunable platform for optical applications. *Nature Chemistry*, 2(12):1015–1024, 2010.
- [15] Shinji Yamashita. Nonlinear optics in carbon nanotube, graphene, and related 2d materials. *APL Photonics*, 4(3):034301, 2019.
- [16] Nzar Rauf Abdullah, Chi-Shung Tang, Andrei Manolescu, and Vidar Gudmundsson. The interplay of electron-photon and cavity-environment coupling on the electron transport through a quantum dot system. *Physica E: Low-dimensional Systems and Nanostructures*, 119:113996, 2020.
- [17] Nzar Rauf Abdullah. Rabi-resonant and intraband transitions in a multilevel quantum dot system controlled by the cavity-photon reservoir and the electron-photon coupling. *Results in Physics*, 15:102686, 2019.
- [18] F. Schedin, A. K. Geim, S. V. Morozov, E. W. Hill, P. Blake, M. I. Katsnelson, and K. S. Novoselov. Detection of individual gas molecules adsorbed on graphene. *Nature Materials*, 6(9):652–655, 2007.
- [19] Myron D. Kapetanakis, Wu Zhou, Mark P. Oxley, Jaekwang Lee, Micah P. Prange, Stephen J. Pennycook, Juan Carlos Idrobo, and Sokrates T. Pantelides. Low-loss electron energy loss spectroscopy: An atomic-resolution complement to optical spectroscopies and application to graphene. *Phys. Rev. B*, 92:125147, Sep 2015.
- [20] Pooja Rani, Girija S. Dubey, and V.K. Jindal. Dft study of optical properties of pure and doped graphene. *Physica E: Low-dimensional Systems and Nanostructures*, 62:28 – 35, 2014.
- [21] Masayuki Kawaguchi, Tadayuki Kawashima, and Tsuyoshi Nakajima. Syntheses and structures of new graphite-like materi-

- als of composition bcn(h) and bc3n(h). *Chemistry of Materials*, 8(6):1197–1201, 1996.
- [22] Yushi Yokomizo and Jun Nakamura. Giant seebeck coefficient of the graphene/h-bn superlattices. *Applied Physics Letters*, 103(11):113901, 2013.
- [23] J. P. Perdew and Alex Zunger. Self-interaction correction to density-functional approximations for many-electron systems. *Phys. Rev. B*, 23:5048–5079, May 1981.
- [24] D. R. Hamann, M. Schlüter, and C. Chiang. Norm-conserving pseudopotentials. *Phys. Rev. Lett.*, 43:1494–1497, Nov 1979.
- [25] W. Kohn and L. J. Sham. Self-consistent equations including exchange and correlation effects. *Phys. Rev.*, 140:A1133–A1138, Nov 1965.
- [26] Paolo Giannozzi, Stefano Baroni, Nicola Bonini, Matteo Calandra, Roberto Car, Carlo Cavazzoni, Davide Ceresoli, Guido L Chiarotti, Matteo Cococcioni, Ismaila Dabo, et al. Quantum espresso: a modular and open-source software project for quantum simulations of materials. *Journal of physics: Condensed matter*, 21(39):395502, 2009.
- [27] Paolo Giannozzi, Oliviero Andreussi, Thomas Brumme, Oana Bunau, M Buongiorno Nardelli, Matteo Calandra, Roberto Car, Carlo Cavazzoni, Davide Ceresoli, Matteo Cococcioni, et al. Advanced capabilities for materials modelling with quantum espresso. *Journal of Physics: Condensed Matter*, 29(46):465901, 2017.
- [28] Anton Kokalj. Xcrysdena new program for displaying crystalline structures and electron densities. *Journal of Molecular Graphics and Modelling*, 17(3):176 – 179, 1999.
- [29] R. de L. Kronig. On the theory of dispersion of x-rays. *J. Opt. Soc. Am.*, 12(6):547–557, Jun 1926.
- [30] Georg KH Madsen and David J Singh. Boltztrap. a code for calculating band-structure dependent quantities. *Computer Physics Communications*, 175(1):67–71, 2006.
- [31] Hunar Omar Rashid, Nzar Rauf Abdullah, and Vidar Gudmundsson. Silicon on a graphene nanosheet with triangle- and dot-shape: Electronic structure, specific heat, and thermal conductivity from first-principle calculations. *Results in Physics*, 15:102625, 2019.
- [32] Nzar Rauf Abdullah, Hunar Omar Rashid, Mohammad T. Kareem, Chi-Shung Tang, Andrei Manolescu, and Vidar Gudmundsson. Effects of bonded and non-bonded b/n codoping of graphene on its stability, interaction energy, electronic structure, and power factor. *Physics Letters A*, 384(12):126350, 2020.
- [33] A. D. Becke and K. E. Edgecombe. A simple measure of electron localization in atomic and molecular systems. *The Journal of Chemical Physics*, 92(9):5397–5403, 1990.
- [34] Yan Gao, Haifeng Wang, Maozhu Sun, Yingchun Ding, Lichun Zhang, and Qingfang Li. First-principles study of intrinsic phononic thermal transport in monolayer c3n. *Physica E: Low-dimensional Systems and Nanostructures*, 99:194 – 201, 2018.
- [35] Xiaofeng Fan, Zexiang Shen, A. Q. Liu, and Jer-Lai Kuo. Band gap opening of graphene by doping small boron nitride domains. *Nanoscale*, 4:2157–2165, 2012.
- [36] L.A. Falkovsky. Symmetry constraints on phonon dispersion in graphene. *Physics Letters A*, 372(31):5189 – 5192, 2008.
- [37] Shunhong Zhang, Jian Zhou, Qian Wang, Xiaoshuang Chen, Yoshiyuki Kawazoe, and Puru Jena. Penta-graphene: A new carbon allotrope. *Proceedings of the National Academy of Sciences*, 112(8):2372–2377, 2015.
- [38] Bohayra Mortazavi and Gianauelio Cuniberti. Atomistic modeling of mechanical properties of polycrystalline graphene. *Nanotechnology*, 25(21):215704, may 2014.
- [39] Changgu Lee, Xiaoding Wei, Jeffrey W. Kysar, and James Hone. Measurement of the elastic properties and intrinsic strength of monolayer graphene. *Science*, 321(5887):385–388, 2008.
- [40] Rassin Grantab, Vivek B. Shenoy, and Rodney S. Ruoff. Anomalous strength characteristics of tilt grain boundaries in graphene. *Science*, 330(6006):946–948, 2010.
- [41] Chung-Huai Chang, Xiaofeng Fan, Lain-Jong Li, and Jer-Lai Kuo. Band gap tuning of graphene by adsorption of aromatic molecules. *The Journal of Physical Chemistry C*, 116(25):13788–13794, 2012.
- [42] Jun Zhu, Sumanta Bhandary, Biplab Sanyal, and Henrik Ottosson. Interpolation of atomically thin hexagonal boron nitride and graphene: Electronic structure and thermodynamic stability in terms of all-carbon conjugated paths and aromatic hexagons. *The Journal of Physical Chemistry C*, 115(20):10264–10271, 2011.
- [43] Santanu Sarkar, Elena Bekyarova, and Robert C. Haddon. Covalent chemistry in graphene electronics. *Materials Today*, 15(6):276 – 285, 2012.
- [44] Sumanta Bhandary and Biplab Sanyal. Graphene-boron nitride composite: A material with advanced functionalities. 2012.
- [45] Ramachandran Rakhi and Cherumuttathu H. Suresh. A dft study on dihydropyrazine annulated linear polyacenes: aromaticity, stability and homolumo energy modulation. *Phys. Chem. Chem. Phys.*, 18:24631–24641, 2016.
- [46] Philippe Dollfus, Viet Hung Nguyen, and Jérôme Saint-Martin. Thermoelectric effects in graphene nanostructures. *Journal of Physics: Condensed Matter*, 27(13):133204, mar 2015.
- [47] V. G. Kravets, A. N. Grigorenko, R. R. Nair, P. Blake, S. Anisimova, K. S. Novoselov, and A. K. Geim. Spectroscopic ellipsometry of graphene and an exciton-shifted van hove peak in absorption. *Phys. Rev. B*, 81:155413, Apr 2010.
- [48] T. Eberlein, U. Bangert, R. R. Nair, R. Jones, M. Gass, A. L. Bleloch, K. S. Novoselov, A. Geim, and P. R. Briddon. Plasmon spectroscopy of free-standing graphene films. *Phys. Rev. B*, 77:233406, Jun 2008.
- [49] Georg K. H. Madsen and David J. Singh. Boltztrap. a code for calculating band-structure dependent quantities. *Computer Physics Communications*, 175(1):67–71, 2006.
- [50] S. Das Sarma and E. H. Hwang. Density-dependent electrical conductivity in suspended graphene: Approaching the dirac point in transport. *Phys. Rev. B*, 87:035415, Jan 2013.
- [51] Nathaniel M. Gabor, Justin C. W. Song, Qiong Ma, Nityan L. Nair, Thiti Taychatanapat, Kenji Watanabe, Takashi Taniguchi, Leonid S. Levitov, and Pablo Jarillo-Herrero. Hot carrier-assisted intrinsic photoresponse in graphene. *Science*, 334(6056):648–652, 2011.
- [52] Justin C. W. Song, Mark S. Rudner, Charles M. Marcus, and Leonid S. Levitov. Hot carrier transport and photocurrent response in graphene. *Nano Letters*, 11(11):4688–4692, 2011. PMID: 21936568.
- [53] Koichi Saito, Jun Nakamura, and Akiko Natori. Ballistic thermal conductance of a graphene sheet. *Phys. Rev. B*, 76:115409, Sep 2007.
- [54] Kin Chung Fong, Emma E. Wollman, Harish Ravi, Wei Chen, Aashish A. Clerk, M. D. Shaw, H. G. Leduc, and K. C. Schwab. Measurement of the electronic thermal conductance channels and heat capacity of graphene at low temperature. *Phys. Rev. X*, 3:041008, Oct 2013.
- [55] S. Yien and A. R. Champagne. Wiedemannfranz relation and thermal-transistor effect in suspended graphene. *Nano Letters*, 14(1):289–293, 2014. PMID: 24341325.
- [56] Nzar Rauf Abdullah, Chi-Shung Tang, Andrei Manolescu, and Vidar Gudmundsson. Thermoelectric inversion in a resonant quantum dot-cavity system in the steady-state regime. *Nanomaterials*, 9(5), 2019.
- [57] Nzar Rauf Abdullah and Vidar Gudmundsson. Single-photon controlled thermospin transport in a resonant ring-cavity system. *Physica E: Low-dimensional Systems and Nanostructures*, 104:223 – 228, 2018.